A hole-transport material that also passivates perovskite surface defects for solar cells with improved efficiency and stability

Journal:	*Energy & Environmental Science*
Manuscript ID	EE-ART-05-2020-001655.R2
Article Type:	Paper
Date Submitted by the Author:	13-Sep-2020
Complete List of Authors:	ZHAO, XIAOMING; Princeton University, Department of Chemical & Biological Engineering Yao, Chao; Princeton University, Department of Chemical Engineering Gu, Kaichen; Princeton University, Chemical and Biological Engineering Liu, Tianran; Princeton University, Department of Electrical Engineering Xia, Yu; Princeton University, Department of Chemical Engineering Loo, Yueh-Lin; Princeton University, Department of Chemical Engineering

SCHOLARONE™
Manuscripts

A hole-transport material that also passivates perovskite surface defects for solar cells with improved efficiency and stability

By Xiaoming Zhao[1], Chao Yao[1,#], Kaichen Gu[1], Tianran Liu[1], Yu Xia[1] and Yueh-Lin Loo[1,2,]*

[1] Department of Chemical and Biological Engineering, Princeton University, Princeton, New Jersey 08544, United States.
[2] Andlinger Center for Energy and the Environment, Princeton University, Princeton, New Jersey 08544, United States.
* Corresponding author: Yueh-Lin Loo (Email: lloo@princeton.edu)
# Present address: School of Advanced Materials, Peking University Shenzhen Graduate School, Shenzhen, 518055 China.

Keywords: perovskite solar cells; hole-transport materials; dopant-free; surface passivation.

Abstract: While typical perovskite solar cells (PSCs) with doped Spiro-OMeTAD as hole transport material (HTM) have shown rapid increase in their power-conversion efficiencies (PCEs), their poor stability remains a big concern as the dopants and additives used with Spiro-OMeTAD have a strong tendency to diffuse into and degrade the perovskite active layer under normal operating conditions. Aiming to push forward the development of PSCs, many dopant-free small-molecular HTMs have been reported based on energetic considerations for charge transfer and criteria for charge transport. However, the PCEs of state-of-the-art PSCs with dopant-free small-molecular HTMs are still inferior to those using doped Spiro-OMeTAD, and little attention has been paid to the interactions between HTM and perovskite absorber in PSCs. Here, we report a facile design concept to functionalize HTMs so that they can passivate perovskite surface defects and enable perovskite active layers with lower density of surface trap states and more efficient charge transfer to hole transport layer. As a consequence, perovskite solar cells with functionalized HTM exhibit a champion PCE of 22.4%, the highest value for PSCs using dopant-free small molecular HTMs to date, and substantively improved operational stability under continuous illumination. With a T_{80} of (1617 ± 7) h for encapsulated cells tested at 30 °C in air, the PSCs containing functionalized HTM are among the most stable PSCs using dopant-free small-molecular HTMs. The effectiveness of our strategy is demonstrated in PSCs comprising both a state-of-the-art MA-free perovskite and MAPbI, a system having more surface defects, and implies the potential generality of our strategy for a broad class of perovskite systems, to further advance highly efficient and stable solar cells.

Introduction

Metal halide perovskite solar cells (PSCs) have attracted much attention due to the rapid increase in their power-conversion efficiencies (PCEs), and the promise that they can be solution processed at low cost.[1] Since Miyasaka *et al.* first introduced perovskites to photovoltaic cells to obtain an efficiency of 3.8% in 2009, the efficiency of PSCs has dramatically improved to over 25% through the development of new functional materials and the optimization of devices fabrication and processing methods, such as composition engineering of the perovskite active layer and interface engineering at the electrodes.[2–14] PSCs rely on hole-transport materials (HTMs) to efficiently extract holes from the perovskite active layer and suppress charge recombination at the anode.[15,16] As a crucial part of state-of-the-art n-i-p-type PSCs, 2,2′,7,7′-tetrakis(*N,N*-di-*p*-methoxyphenylamino)-9,9′-spirobifluorene, or Spiro-OMeTAD, has become the most widely-used HTM in PSCs that exhibit high efficiencies.[4,17–20] However, this HTM only effective when it is doped with metal complexes and/or additives such as Li-TFSI and *t*-BP. Since these dopants and additives have a strong tendency to diffuse into and degrade the perovskite active layer under normal operating conditions, the incorporation of doped Spiro-OMeTAD has affected the long-term stability of PSCs, in essence trading long-term stability for short-term performance gains.[21–23] On the other hand, doped HTMs without Li-TFSI, such as EH44/EH44-ox, have resulted in PSCs with excellent operational stability, but their PCEs are low, reflecting constraints by the same stability and efficiency trade-off.[24] Developing dopant-free HTMs that can enable PSCs with high stability without sacrificing cell efficiency has thus become an important topic. As a side benefit, dopant-free HTMs can also simplify device fabrication and processing, with fewer material requirements and potentially lower manufacturing costs.

Aiming to push forward the development of PSCs, many dopant-free HTMs have been reported based on energetic considerations for charge transfer and criteria for charge transport. The energy level of the highest occupied molecular orbital (HOMO) of the HTM should, for example, be higher than that of the perovskite active layer in order for holes to transfer effectively across the perovskite/hole-transport layer (HTL) interface. Further, the HTM should have a relatively high hole mobility ($>10^{-4}$ cm^2 V^{-1} s^{-1}) in its pristine form so dopants and additives are not needed to facilitate the transport of holes to the anode in order to maintain stable device operation. Importantly, an ideal HTM should be accessed by facile, simple and scalable synthesis and purification. It is for the last reason that small-molecule HTMs are of particular interest as the

synthesis of small-molecule alternatives – as opposed to their polymer counterparts – can be more precisely controlled, yielding chemically purer and structurally more homogeneous products that would ultimately lead to more uniform properties and more reproducible PSCs.[10,25–29] Although these design rules are well known, the PCE of PSCs with small-molecule HTM alternates remains below that of PSCs having doped Spiro-OMeTAD. At 21%, the highest PCE of PSCs with a small-molecule dopant-free HTM, in this case, DTP-C6Th, is almost 1% lower than that of otherwise analogous PSCs using Spiro-OMeTAD.[30] This and other examples in the literature suggest room for further development of dopant-free HTM to realize highly efficient and stable PSCs.

On the other hand, recent studies have revealed that defects – especially in the form of under-coordinated lead – exist at the surface of solution-processed perovskite thin films.[29,31] Present at the interface between the perovskite active layer and the HTL, these defects act as charge-carrier recombination centers to hinder charge transfer from perovskite to HTL.[29] In addition, the presence of under-coordinated lead can accelerate the degradation of PSCs under continuous illumination.[32] To address this challenge, interlayers have been introduced between the perovskite active layer and the HTL to passivate these surface defects.[7,33–39] Among them, two-dimensional (2D) perovskites, formed in-situ on three-dimensional (3D) perovskite surfaces (the so-called "2D/3D stacked perovskites"), is the most widely-used strategy to passivate 3D perovskite surface defects. However, there are two drawbacks of these interlayers: i) the formation of 2D perovskite atop 3D perovskite is very sensitive to the deposition conditions and require local compositional drifts to avoid impure 2D perovskite phases across the bulk perovskite absorber;[19,35,40] ii) 2D perovskites are often wider in bandgap and contain insulating alkyl ligands which could hinder charge transfer and impede hole transport from the 3D perovskite active layer to the HTL. Therefore, these interlayers need to be very thin to allow carriers to tunnel across them, which further complicates device fabrication.

One possible solution to the challenges outlined above is to develop HTMs with dual functionalities, one that can simultaneously passivate perovskite surface defects while presenting suitable HOMO energy levels and hole mobilities to facilitate interfacial charge transfer so PSCs can maintain high efficiencies without sacrificing operation stability. While this concept has been demonstrated in inverted-architecture p-i-n PSCs in which the HTMs are beneath the perovskite absorbers,[41,42] the achieved PCEs are still moderate and there has been no such demonstration of HTM that can passivate perovskite surface in state-of-the-art conventional-architecture n-i-p PSCs

in which the HTM is deposited atop the perovskite absorber. To demonstrate this concept, we designed and synthesized two compounds with dianisylphenylamine side groups and either phenanthrene (YZ18) or 1,10-phenanthroline (YZ22) as the conjugated core, and evaluated them as HTM alternatives to Spiro-OMeTAD for PSCs. The synthesis and purification of YZ18 and YZ22 are simple and facile at gram-scale quantities. The chemical structures of YZ18 and YZ22 are similar and they both exhibit similar and suitable HOMO energy levels and hole mobilities to be used as HTMs for PSCs. When these compounds are incorporated as HTMs in PSCs, the outcome is surprisingly different. $Cs_{0.1}FA_{0.9}PbI_3$ (CsFAPbI) PSCs with YZ22 exhibit a champion PCE of 22.4%, not only significantly higher than otherwise analogous solar cells comprising YZ18 (18.1%), but also the highest among PSCs using small molecular dopant-free HTMs (**Table S1**). Characterizations by grazing-incidence wide-angle X-ray scattering (GIWAXS), Fourier-transform infrared spectroscopy (FTIR) and X-ray photoelectron spectroscopy (XPS) reveal interfacial coordination between under-coordinated lead at the CsFAPbI surface with YZ22; this coordination effectively passivates surface defects and enhances interfacial hole extraction, effectively boosting the solar-cell performance of devices that incorporate YZ22. While PSCs with YZ18 and YZ22 both show better operational stability compared to PSC using doped Spiro-OMeTAD, we found surface passivation by YZ22 to further improve the operational stability of these PSCs. With an estimated average T_{80} of (1617 ± 7) h for encapsulated cells tested at 30 °C in air, under MPP tracking conditions with a constant 1.1-sun illumination, the PSC containing YZ22 is among the most stable PSCs using dopant-free HTMs. Finally, we demonstrate the effectiveness of our strategy on solar cells based on $MAPbI_3$ (MAPbI), a perovskite materials system with yet more surface defects, implicating the potential utility of YZ22 across a broad class of perovskite systems. Our results demonstrate the effectiveness of multi-functional HTMs to advance highly efficient and stable perovskite solar cells and provide a critical design concept for future HTM engineering.

Results and Discussions

1,10-phenanthroline is a widely-used ligand in coordination chemistry, forming strong complexes with metal ions, including Pb^{2+}.[43] With an ambition to passivate uncoordinated Pb ions at the surfaces of perovskite active layers, we chose 1,10-phenanthroline as the conjugated core for the construction of a multi-functional HTM, 4,4'-(1,10-phenanthroline-3,8-diyl)bis(N,N-bis(4-

methoxyphenyl)aniline), which we refer to as YZ22. As control, we also designed an analogous HTM, 4,4'-(phenanthrene-2,7-diyl)bis(N,N-bis(4-methoxyphenyl)aniline), named YZ18, whose conjugated core is phenanthrene instead of 1,10-phenanthroline. While structurally similar, phenanthrene has no tendency to coordinate with Pb^{2+}. We successfully synthesized YZ18 and YZ22 (chemical structures in **Figure 1a**) by one-step Suzuki coupling reactions (synthetic routes and details can be found in **Figure S1** and **Experimental Section**). Their structures were independently verified by [1]H- and ^{13}C nuclear magnetic resonance (NMR) and mass spectra (**Figure S2-S4**). We determined their optical bandgaps and energy levels by ultraviolet-visible absorption spectroscopy (**Figure 1b**) and ultraviolet photoelectron spectroscopy (UPS, **Figure S5**). We found both compounds to present suitable HOMO energy levels (-5.26 and -5.20 eV for YZ18 and YZ22, respectively) to be HTMs for PSCs (**Figure 1c**). We determined their hole mobilities by space charge limited current (SCLC) method according to Child's law (**Figure 1d, Table 1**). YZ18 and YZ22 exhibit very similar hole mobilities of 9.2 and 8.8×10^{-4} cm^2 V^{-1} s^{-1}, respectively. For reference, these mobilities are more than an order of magnitude higher than that of pristine Spiro-OMeTAD (1.6×10^{-5} cm^2 V^{-1} s^{-1}), and also similar to that of Li-TFSI- and *t*-BP-doped Spiro-OMeTAD (2.6×10^{-4} cm^2 V^{-1} s^{-1}; with molar ratios of Li-TFSI and t-BP to Spiro-OMeTAD of 2.0 and 0.5, respectively).[44] From the perspectives of energy levels and mobility, YZ18 and YZ22 thus appear to be appropriate and comparable dopant-free HTM alternatives for PSCs. We then fabricated and characterized PSCs with either YZ18 or YZ22 as the HTL. To demonstrate, we chose to work with a methylammonium (MA)-free perovskite of $Cs_{0.1}FA_{0.9}PbI_3$ (CsFAPbI) as the absorber in our PSCs due to its higher chemical stability in precursor solutions and as thin films in solar cells compared to MA-containing compositions.[45–47] Interestingly, we found PSCs based on YZ18 and YZ22 to perform differently despite the similarities in their chemical structures and properties (**Figure 1e-f, Figure S6-S7**). CsFAPbI PSCs with YZ22 as the HTL exhibit a champion PCE of 22.4%, significantly higher than that with YZ18 (18.1%) and is the highest among PSCs with dopant-free small-molecular HTMs (**Table S1**), making YZ22 a promising alternative for highly efficient PSCs. The performance enhancement of YZ22-based PSC stems from improved open-circuit voltage (V_{OC}) and fill factor (FF).

To understand the origins of this performance enhancement and to verify our hypothesis that YZ22 plays multiple roles in PSCs, we first employed GIWAXS to investigate the interface between YZ22 and CsFAPbI (**Figure 2, Figure S8**). GIWAXS patterns of YZ22 (**Figure 2a**) and

YZ18 (**Figure S8**) films exhibit a weak diffuse halo, implying the lack of long-range order in these films. The GIWAXS pattern of CsFAPbI exhibits characteristic Bragg reflections belonging to the cubic phase of CsFAPbI (**Figure 2b**). With HTMs atop CsFAPbI, the Bragg reflections in these GIWAX patterns corresponding to CsFAPbI are invariant, suggesting the deposition of either YZ18 or YZ22 atop CsFAPbI does not change the bulk perovskite crystal structure. We do not observe any additional reflections in the GIWAXS pattern of the stack comprising YZ18 on CsFAPbI (**Figure S8**). In contrast, we observe unique, new reflections in the GIWAXS pattern of the stack comprising YZ22 on CsFAPbI, which suggest additional structuring in the stack (**Figure 2c**). **Figure 2d and 2e** present the out-of-plane line cuts (q vector along in-plane, that is $q_{xy} = 0$) of these GIWAXS profiles. We find these new reflections appear at q_z (q vector along out-of-plane) smaller than those associated with the reflections of the cubic phase of CsFAPbI; the characteristic distance of this newly emerged structure must be larger than those between the lattice planes of cubic CsFAPbI. Separate attempts to grow single crystals of YZ22 with PbI_2 led to the discovery of an orange precipitate, even at 0.001M solids concentration in DMF. Such precipitate is not observed when YZ18 is mixed with PbI_2 in DMF (**Figure S9**). While these crystals were too small to be resolved by single-crystal XRD, the formation of the orange precipitate suggests strong complexation that is unique to YZ22 and PbI_2. Powder XRD on the precipitate reveals a reflection at $2\theta = 9.5°$, which matches the strong reflection in the XRD pattern of CsFAPbI/YZ22, which suggests that we are accessing the same YZ22/PbI_2 complex in the CsFAPbI/YZ22 stack.

To further investigate the nature of this interaction, we performed XPS depth profiling of Pb 4f core level on CsFAPbI, stacks comprising 10 nm of YZ18 on CsFAPbI, and 10 nm of YZ22 on CsFAPbI (**Figure 3a-c**). The HTL were 80-nm thick in full devices; this same thickness was used for absorption, GIWAXS, SCLC, UPS, as well as FTIR and PL studies. The thickness of HTL was only 10 nm for XPS studies because these thinner films allowed us to probe the CsFAPbI/HTL interface more easily. The ion beam sputtering conditions were optimized following reports in the literature to avoid damage.[48] The XPS spectra of YZ18 on CsFAPbI and of CsFAPbI show main peaks corresponding to fully coordinated Pb^{2+} (138.3 eV for $4f_{7/2}$ and 143.2 eV for $4f_{5/2}$) and also show smaller peaks at lower binding energy (136.8 eV for $4f_{7/2}$ and 141.7 eV for $4f_{5/2}$). Snaith *et al* also observed these smaller peaks at lower binding energy from pristine perovskite films and attributed these peaks to the presence of under-coordinated Pb ions as highly under-coordinated Pb ions may show metallic character.[49–51] In contrast, we observe a marked

difference in the electronic environment of Pb in the XPS spectrum of YZ22 on CsFAPbI. In this spectrum, we only see peaks associated with fully coordinated Pb^{2+}; peaks attributed to under-coordinated Pb^{2+} are absent. Comparison of the XPS spectra indicates qualitative differences at the HTM-CsFAPbI interface, and suggests YZ22 to coordinate with under-coordinated Pb ions at the CsFAPbI surface. To further confirm the interaction between YZ22 and CsFAPbI, we studied the XPS spectra of the I 3d region of these three samples in (**Figure S10** in supporting information). We find the I $3d_{3/2}$, $3d_{5/2}$ signals in the XPS spectrum for CsFAPbI/YZ22 to shift to lower binding energy compared to those in the XPS spectrum of neat CsFAPbI and CsFAPbI/YZ18. We believe this shift to stem from YZ22 donating electrons to Pb^{2+}, which perturbs the static interactions between Pb^{2+} and I^- at the interface. To verify that our observation is limited to the perovskite-HTL interface of interest, we analyzed the XPS depth profiles of O 1s core level of 10-nm YZ22 on CsFAPbI (**Figure S11**). Its spectrum shows oxygen atoms, which are unique to YZ22, are only present in the top 10 nm depth, an observation we took to indicate that YZ22 is only present at the surface and does not diffuse into the bulk of CsFAPbI.

We performed attenuated total reflectance-FTIR (ATR-FTIR) on YZ22, CsFAPbI and a stack of YZ22 on CsFAPbI (**Figure S12**) to elucidate the nature of interaction between these two species. In the spectrum of neat YZ22, characteristic 1,10-phenanthroline bands, related with ring vibrations, are observed at 1213, 1141, 1100 and 1037 cm^{-1}.[52–55] In the spectrum taken of YZ22 on CsFAPbI, the bands at 1141, 1100 and 1037 cm^{-1} shift to 1144, 1110 and 1031 cm^{-1}, respectively, while the band at 1213 cm^{-1} splits into two, each located at 1218 and 1205 cm^{-1}. According to the literature, these changes suggest interaction of 1,10-phenanthroline with under-coordinated Pb^{2+} (**Figure 3d**),[52–55] further adding evidence to support our XPS analyses that reveal an elimination of under-coordinated Pb^{2+} when YZ22 is introduced to the perovskite surface.

Next, we employed photoluminescence (PL) spectroscopy to investigate the effect of this coordination on interface charge-carrier dynamics. PL excitation wavelength in our measurements was set as 520 nm which is transparent to both YZ18 and YZ22 (**Figure 1b**). **Figure 4a** shows the steady-state PL spectra of neat CsFAPbI film, of YZ18 on CsFAPbI and of YZ22 on CsFaPbI, excited from the glass side (more bulk sensitive). These PL spectra are comparable, implying that the quality of CsFAPbI that is closer to the glass substrate is not affected by the deposition of the HTM top layer. Interestingly, the PL spectra of these three samples exhibit characteristically different PL intensities when the films are excited from the surface (more surface sensitive). Neat

CsFAPbI exhibits strong PL intensity; after the deposition of HTMs atop CsFAPbI, the PL intensity decreases significantly (**Figure 4b**). At steady state, the PL intensity is directly related to quasi-Fermi level splitting.[56] The quasi-Fermi level splitting will depend on the illumination conditions, the Shockley-Read-Hall (SRH) lifetime, the pre-factor of recombination, and the equilibrium concentration of charge carriers.[56] In perovskites, the nonradiative processes that occur through defect-assisted recombination (mainly SRH recombination) may occur in the bulk, at grain boundaries, and at interfaces with other layers, such as the HTL.[56] That CsFAPbI/YZ22 exhibits a lower PL intensity than CsFAPbI/YZ18 could stem from more efficient hole extraction at the CsFAPbI/YZ22 interface, and/or more serious nonradiative recombination in the bulk of CsFAPbI, or at the CsFAPbI/YZ22 interface. Since GIWAXS patterns indicate that the long-range order of CsFAPbI is comparable when either YZ22 or YZ18 is deposited atop, we believe the bulk structure of CsFAPbI to be unaltered by the deposition of the HTM. We are thus left to surmise that the lower PL in CsFAPbI/YZ22 can stem from more efficient hole extraction by YZ22 and/or more serious nonradiative recombination at the CsFAPbI/YZ22 interface. To better understand, we employed time-resolved PL (TRPL) to study the charge-carrier dynamics in CsFAPbI/HTL samples with excitation and detection wavelength being 526 nm and 800 nm, respectively. **Figure 4c** shows the TRPL spectra of glass/CsFAPI and glass/CsFAPI/HTL (YZ18 or YZ22) samples. The PL of CsFAPbI on glass decays monoexponentially and can be described by *eqn. 1*: [57]

$$f(t) = A \, exp\left(-\frac{t}{\tau}\right) + B \quad (1)$$

where τ is decay time constants, A is its corresponding decay amplitudes, and B is a constant. The corresponding decay time of this sample is 490 ns. With the deposition of HTL (YZ18 or YZ22) atop CsFAPbI, the TRPL transients show a bi-exponential decay with a relatively fast initial decay followed by a subsequent slower decay. We fitted these TRPL curves with a biexponential decay function (*eqn. 2*): [58]

$$f(t) = A_1 \, exp\left(-\frac{t}{\tau_1}\right) + A_2 \, exp\left(-\frac{t}{\tau_2}\right) + B \quad (2)$$

where τ_1 and τ_2 are the fast and slow decay time constants, respectively, A_1 and A_2 are their corresponding decay amplitudes, and B is a constant. The presence of a fast initial decay in the PL transient spectra of CsFAPbI with HTL suggests efficient charge transfer (rather than detrimental recombination) in addition to a slower decay that can be attributed to charge recombination.[59–61] The glass/CsFAPbI/YZ22 sample exhibits a much faster initial decay with τ_1 of 14 ns, which is

significantly shorter than that of glass/CsFAPbI/YZ18 (57 ns), implying YZ22 is likely to be more efficient at extracting charges from CsFAPbI than YZ18. Interestingly, τ_2 of glass/CsFAPbI/YZ22 is 686 ns; this lifetime is not only longer than that of glass/CsFAPbI/YZ188 (478 ns), but it also surpasses the carrier lifetime of glass/CsFAPbI (490 ns). This substantively increased carrier lifetime implies successful suppression of charge recombination with YZ22 atop the perovskite absorber, consistent with our observations of the steady state of these samples when they are excited from the film side. **Figure S13** presents the PL spectra of these samples excited from the film side with their y-axes normalized to their maximum PL intensities. In particular, the PL of CsFAPbI/YZ22 exhibits a narrower and 5-nm blue-shift in its emission compared with those of neat CsFAPbI and CsFAPbI/YZ18, implying the successful passivation of CsFAPbI surface defects with YZ22.[62,63] This set of analyses further confirms the dual functionality of YZ22. Not only can it provide a means to efficiently extract charges from CsFAPbI, it also effectively passivates the surface defects of the perovskite absorber to reduce the density of surface traps and enhance carrier lifetimes, accounting for the enhanced V_{OC} in solar cells with YZ22.[25,64–68]

A successful HTM candidate should not compromise long-term stability for short-term performance gains of the device. PSCs with dopant-free HTMs have been reported to show superior stability compared to those with LiTFSI-doped Spiro-OMeTAD, given the absence of dopants and additives in these HTMs, but these cells suffer lower efficiency compared to cells with LiTFSI-doped Spiro-OMeTAD.[10,25–29] Although PSCs using doped HTMs without LiTFSI can achieve excellent operational stability, the same trade-off exists with regard to stability/efficiency.[24,69] It was unclear, however, whether the interfacial coordination between YZ22 and CsFAPbI would further improve device stability without sacrificing cell efficiency. **Figure 4d** tracks the PCE to quantify the operational stability of encapsulated CsFAPbI devices with YZ18, YZ22 and doped Spiro-OMeTAD as HTM under continuous 1.1-sun illumination in ambient air (ca. ~30 °C, ~35% R.H.).[70] Average values and standard deviations were obtained from 5 devices at each condition. We observe that PSCs using dopant-free HTMs (YZ18 or YZ22) are much more stable than that those with doped Spiro-OMeTAD. On average, the solar cells with YZ22 and YZ18 all retain more than 60 % of their initial PCEs after 1000-hour operation, while the solar cells with doped Spiro-OMeTAD only retain about 10% of their initial PCEs under the same conditions. We attribute this observation to the dopants and additives degrading the perovskite active layer under illumination in the PSC with doped Spiro-OMeTAD.[71] Importantly,

we observe slower degradation with solar cells containing YZ22 than those containing YZ18. On average, the solar cells with YZ22 retain more than 80 % of their initial PCEs after 1000-hour operation, while the solar cells with YZ18 retain 65% of their initial PCEs. To understand this stability improvement, we firstly performed morphological characterization of HTL before and after solar cell stability studies to probe, if any, morphological changes take place. To do so, we mechanically removed the cover slides that encapsulated the aged solar cells and used Scotch tape to peel off the Au electrodes,[32] and conducted SEM of the remaining stacks. As shown in **Figure S14**, we do not observe significant morphological changes that would indicate crystallization or pinhole formation of either HTM films. With these two HTM being structurally similar and their films morphologically similar, we are left to surmise that the significant difference in the stability of solar cells containing them to stem from the only obvious difference between them: YZ22 is able to passivate under-coordinated lead ions while YZ18 is unable to do so. In addition, the PSC using YZ18 shows more severe V_{OC} and *FF* degradation compared with that using YZ22 (**Figure S15** in supporting information). It has been reported that under-coordinated lead at the perovskite/HTL interface can decompose into metallic lead with irradiation.[32,72,73] Metallic Pb can in turn act as a quencher for carriers, which gradually results in charge-carrier recombination as well as ohmic losses at the interface, and can therefore lead to reduced V_{OC} and *FF* during device operation.[32,74,75] Our analyses here suggests that YZ22's ability to passivate under-coordinated lead at the perovskite surface to mainly contribute to the improved operational stability of its corresponding solar cells. Following the method reported by Snaith et al,[76] we also extracted T_{80} values of these PSCs, as shown in **Figure S16,** the average T_{80} of PSCs with YZ22 was estimated to be (1617 ± 7) h, about an order of magnitude higher than that of PSC with doped Spiro-OMeTAD $((185 \pm 2)$ h), and also significantly higher than those with YZ18 $((717 \pm 7)$ h). As shown in **Table S2**, the most stable PSC using dopant-free HTM reported prior to this work is one with FA-CN, which retains 65% of its initial PCE after 1300 hr (unencapsulated cell in Ar atmosphere, 45 °C, MPPT under continuous UV-filtered 1-sun illumination). Our solar cells with YZ22 on average retain 81% of their initial PCE after 1000 hr (encapsulated cell in air, 30 °C, MPPT under continuous 1.1-sun illumination), showing excellent operational stability of YZ22-containing PSCs among PSCs using dopant-free HTM. As shown in **Figure S17**, we also studied the operational stability of PSCs with doped Spiro-OMeTAD or YZ22 as HTL at elevated temperatures. These encapsulated cells were held at MPP at 85 °C in air under an equivalent of

~1.1 sun illumination. Interestingly, although the glass transition temperature (T_g) of YZ22 (108 °C, **Figure S18** in supporting information) is slightly lower than that of Spiro-OMeTAD (126 °C),[77] the devices with YZ22 are more thermally stable compared to those using doped Spiro-OMeTAD, with the latter degrading almost completely after 60 hr while the former maintaining more than 60% of their initial PCEs after the same period. Several reports have shown that the dopants in Spiro-OMeTAD HTL, such as Li-TFSI and *t*-BP, can rapidly degrade the performance of solar cells comprising them at elevated temperatures;[78–82] we thus believe the absence of such dopants in the YZ22 solar cells to improve their thermal stability compared with solar cells comprising doped Spiro-OMeTAD. Our results demonstrate the effectiveness of multi-functional HTMs to achieve both high efficiency and high stability in perovskite solar cells.

Last, we assessed the effectiveness of our strategy on devices based on MAPbI, a perovskite materials system that has more structural defects than CsFAPbI.[32,83–85] Not unlike CsFAPbI, the surface defects of MAPbI are effectively passivated with the deposition of YZ22 (**Figure S19**). By replacing doped Spiro-OMeTAD with YZ22 as HTM, MAPbI solar cells see a PCE improvement from 15.4% to 18.1% (**Figure S20-S21, Table S3).** In addition, the encapsulated solar cell with YZ22 under constant illumination exhibits slower degradation compared to the solar cell with doped Spiro-OMeTAD studied under the same conditions. On average, solar cells with YZ22 retain about 80% of their initial PCE after 300-hour operation while solar cells with doped Spiro-OMeTAD retain less than 20% of their initial PCE after the same period (**Figure S22**). These studies imply the potential generality of our strategy for a broad class of perovskite systems.

Summary

In summary, we have demonstrated a simple yet efficient design concept to advance dopant-free HTMs for perovskite solar cells. Functionalizing HTMs so they can passivate perovskite surface defects enables PSC active layers with lower density of surface trap states and more efficient charge transfer to HTL, which can contribute to substantive improvements in the efficiency and operational stability of solar cells. The effectiveness of our strategy is demonstrated in PSCs comprising both a state-of-the-art MA-free perovskite and MAPbI, a system having more surface defects. The implied generality of our strategy for a broad class of perovskite systems should be

of great benefit for future HTM engineering to further advance highly efficient and stable perovskite solar cells.

Acknowledgements

Competing interests

The authors declare no competing interests.
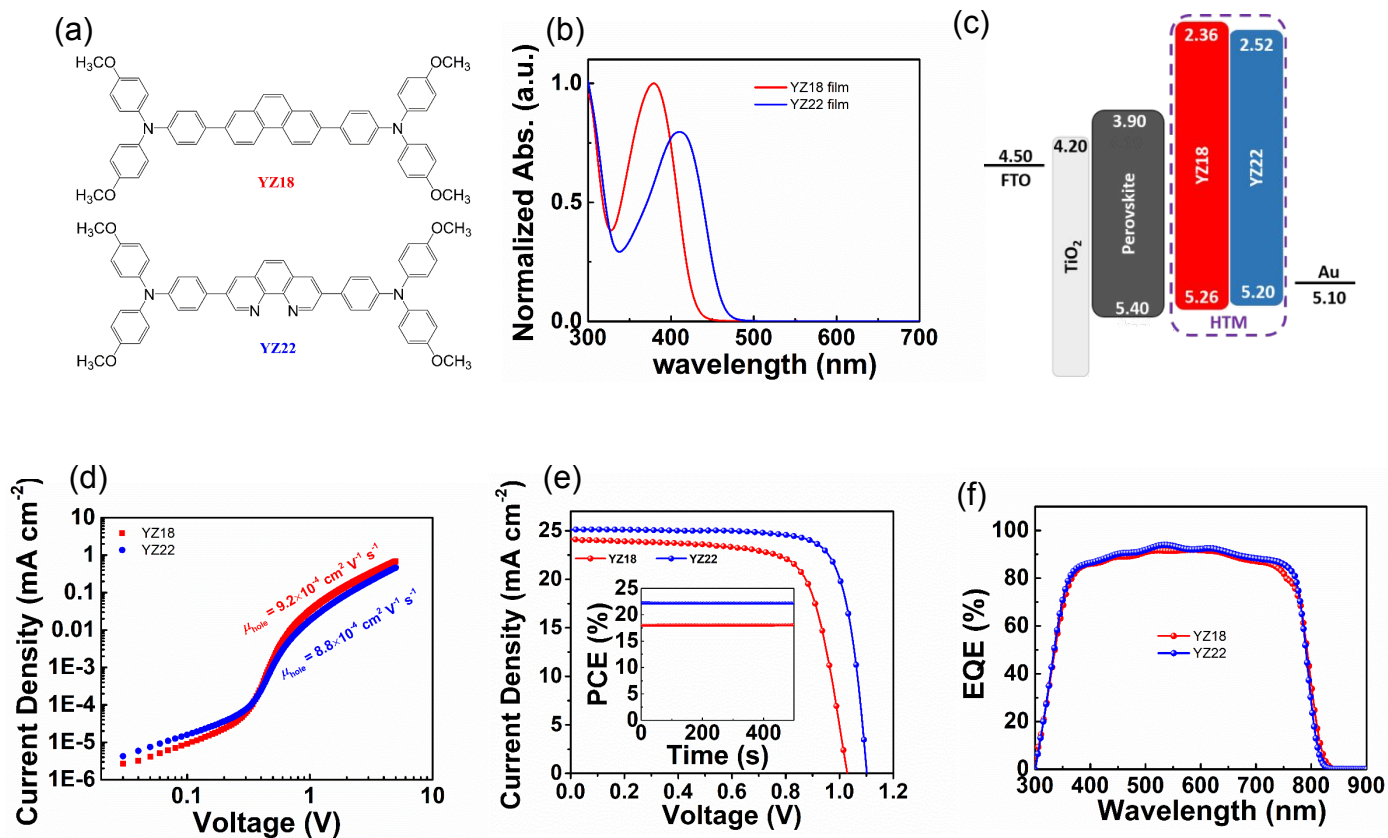
Figure 1. Chemical structures and characterization of new compounds, and their applications as HTM in CsFAPbI-based PSCs. a) Molecular structures, b) UV-vis absorption spectra, c) energy levels and d) hole transport properties of YZ18 and YZ22; e) *J–V* characteristics under reverse scan and steady-state power-conversion efficiency at the maximum power point (PCE_ST, as inset) of CsFAPbI-based PSCs with either YZ18 or YZ22 as HTM; f) EQE of CsFAPbI-based PSCs with either YZ18 or YZ22 as HTM.
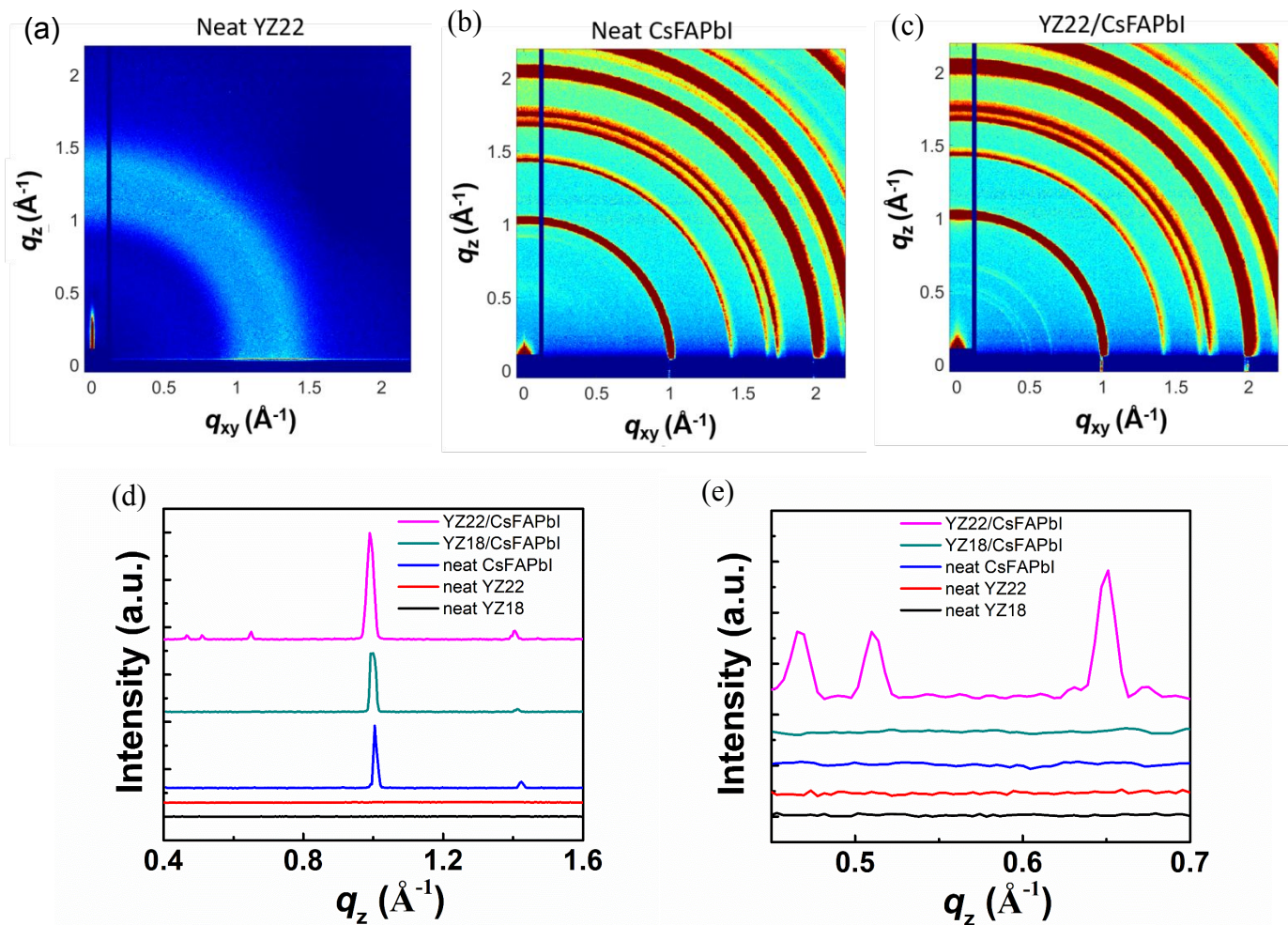
Figure 2. Structural characterization. a-c) GIWAXS patterns of a YZ22 film, a CsFAPbI film, and a stack comprising YZ22 on CsFAPbI. The incident angle during data acquisition is 0.1°; d) Out-of-plane line cuts at $q_{xy} = 0$ of the GIWAXs profiles, including e) magnified traces from GIWAXS patterns.
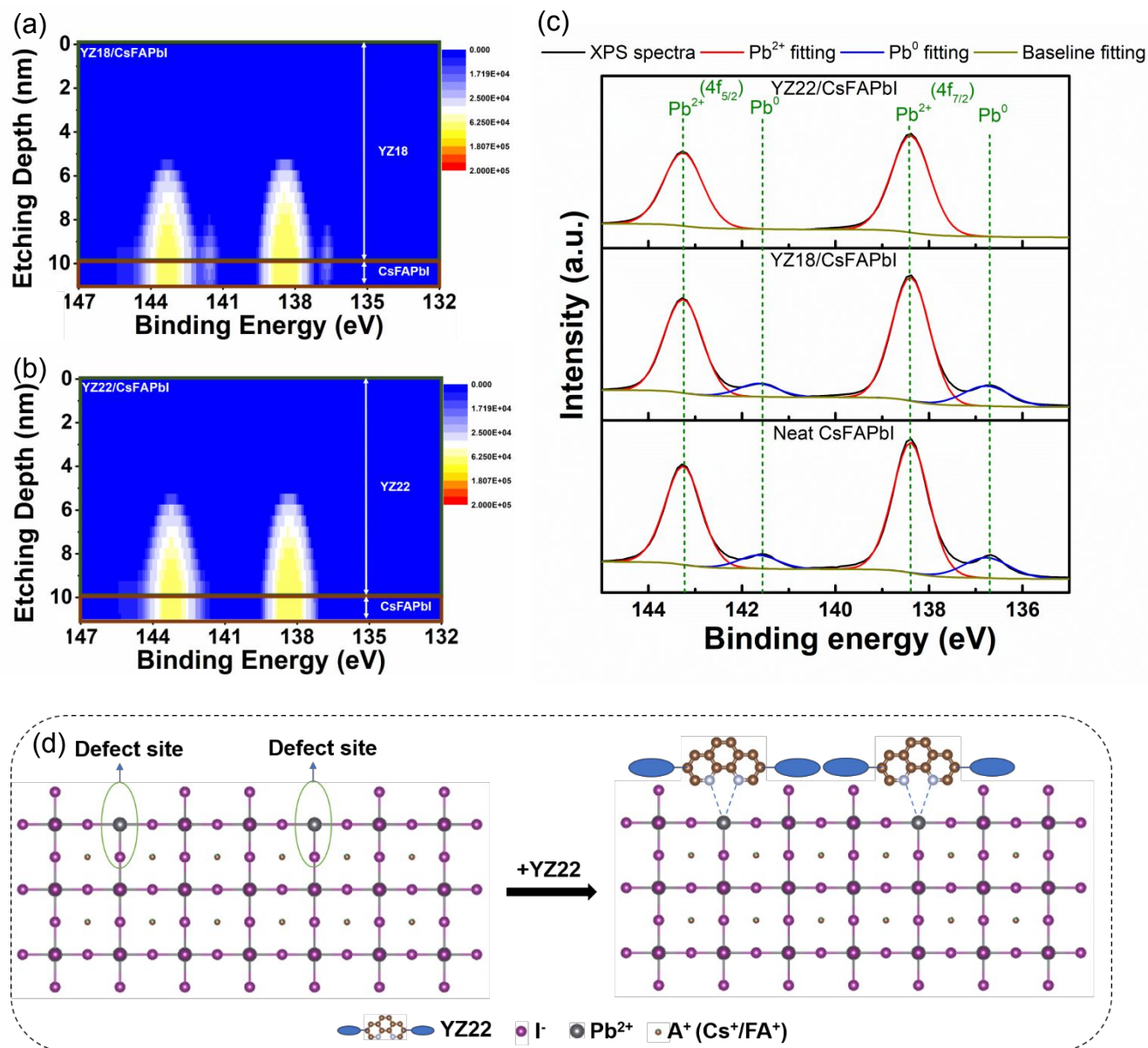
Figure 3. Perovskite surface passivation with YZ22. XPS depth profiling of Pb 4f core level on a) a stack comprising ~10-nm of YZ18 on CsFAPbI and b) a stack comprising ~10-nm thick YZ22 on CsFAPbI; c) XPS of Pb 4f core level of CsFAPbI, of a stack comprising YZ18 on CsFAPbI, and of a stack comprising YZ22 on CsFAPbI. The XPS traces for the stacks were obtained at a depth of 10 nm from the surface; d) representation of how YZ22 passivates under-coordinated lead.
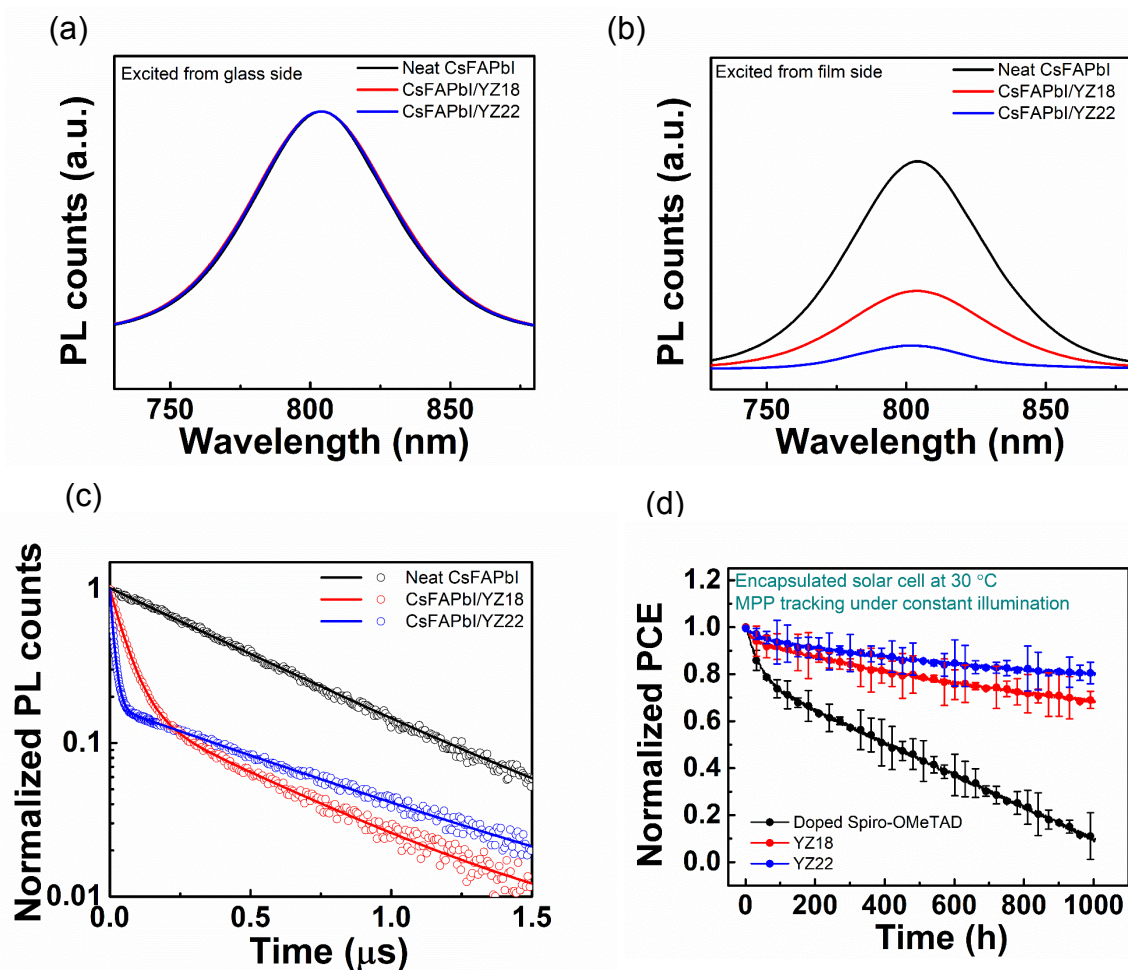
Figure 4. Interfacial charge carrier dynamics of stacks and operation stability of PSCs. Steady-state PL spectra of CsFAPbI, stacks comprising YZ18 on CsFAPbI and YZ22 on CsFAMA excited from a) the glass side, and b) the film side, respectively; c) Time-resolved photoluminescence transient spectra of stacks comprising glass/CsFAPbI (black), glass/CsFAPbI/YZ18 (red), and glass/CsFAPbI/YZ22 (blue); d) Normalized PCE over time for encapsulated devices with doped Spiro-OMeTAD (black), dopant-free YZ18 (red), or dopant-free YZ22 (blue) as HTL that were held at MPP at 30 °C under an equivalent of ~1.1 sun illumination. Average values and standard deviations were obtained from 5 devices studied under each condition.

Table 1. Summary of photophysical and electronic properties of YZ18 and YZ22 films.

HTM	λ_{onset}	$E_g{}^a$	$E_{HOMO}{}^b$	$E_{LUMO}{}^c$	$\mu_h{}^d$
	(nm)	(eV)	(eV)	(eV)	($\times 10^{-4}$ cm^2 V^{-1} s^{-1})
YZ18	427	2.90	-5.26	-2.36	9.0 ± 0.7
YZ22	463	2.68	-5.20	-2.52	8.5 ± 0.6

[a] Calculated from $E_g = (1240/\lambda_{onset})$. [b] Determined from the $E_{cut\text{-}off}$ and $E_V\text{-}E_F$ values from UPS spectra. [c] Determined from $E_{LUMO} = E_{HOMO} + E_g$. [d] Calculated using Child's law, $J = 9\varepsilon_0\varepsilon_T\mu_h V^2/8L^3$, where J is the current density, L is the thickness of the HTM layer, μ_h is the hole mobility, ε_T is the relative dielectric constant of the transport medium, ε_0 is the permittivity of free space (8.85×10^{-12} F m^{-1}), V is the applied voltage to the device (the configuration of hole-only device is Au/HTM/Au). Average and standard deviation values were obtained by measuring 10 devices at the same condition.

Table 2. Summary of the champion and average photovoltaic parameters of CsFAPbI PSCs under reverse voltage scan with either YZ22 or YZ18 as HTM. Parameters followed by * are champion device parameters. Parameters in bracket are average parameters. Average and standard deviation values are obtained by measuring 40 devices for each HTM.

HTM	J_{SC} (mA cm^{-2})	J_{SC} by EQE (mA cm^{-2})	V_{OC} (V)	FF	PCE (%)	PCE$_{ST}$ (%)[a]
YZ18	24.1* (23.5 ± 0.4)	23.5*	1.03* (1.00 ± 0.02)	0.73* (0.72 ± 0.01)	18.1* (17.6 ± 0.3)	18.0*
YZ22	25.1* (24.7 ± 0.4)	24.6*	1.10* (1.09 ± 0.02)	0.81* (0.80 ± 0.01)	22.4* (22.0 ± 0.3)	22.3*

[a] Steady-state power-conversion efficiency at the maximum power point

Reference

1   N. G. Park, M. Grätzel, T. Miyasaka, K. Zhu and K. Emery, *Nat. Energy*, 2016, 1, 16152.

2   NREL, Best Research-Cell Efficiencies, https://www.nrel.gov/pv/assets/pdfs/best-research-cell-efficiencies-190416.pdf.

3   A. Kojima, K. Teshima, Y. Shirai and T. Miyasaka, *J. Am. Chem. Soc.*, 2009, **131**, 6050–6051.

4   H. S. Kim, C. R. Lee, J. H. Im, K. B. Lee, T. Moehl, A. Marchioro, S. J. Moon, R. Humphry-Baker, J. H. Yum, J. E. Moser, M. Grätzel and N. G. Park, *Sci. Rep.*, 2012, **2**, 519.

5   H. Zhou, Q. Chen, G. Li, S. Luo, T. -b. Song, H.-S. Duan, Z. Hong, J. You, Y. Liu and Y. Yang, *Science (80-.).*, 2014, **345**, 542–546.

6   W. S. Yang, B. W. Park, E. H. Jung, N. J. Jeon, Y. C. Kim, D. U. Lee, S. S. Shin, J. Seo, E. K. Kim, J. H. Noh and S. Il Seok, *Science (80-.).*, 2017, **356**, 1376–1379.

7   Q. Jiang, Z. Chu, P. Wang, X. Yang, H. Liu, Y. Wang, Z. Yin, J. Wu, X. Zhang and J. You, *Adv. Mater.*, 2017, **29**, 1703852.

8   Y. Hou, X. Du, S. Scheiner, D. P. McMeekin, Z. Wang, N. Li, M. S. Killian, H. Chen, M. Richter, I. Levchuk, N. Schrenker, E. Spiecker, T. Stubhan, N. A. Luechinger, A. Hirsch, P. Schmuki, H. P. Steinrück, R. H. Fink, M. Halik, H. J. Snaith and C. J. Brabec, *Science (80-.).*, 2017, **358**, 1192–1197.

9   H. Tan, A. Jain, O. Voznyy, X. Lan, F. P. G. De Arquer, J. Z. Fan, R. Quintero-Bermudez, M. Yuan, B. Zhang, Y. Zhao, F. Fan, P. Li, L. N. Quan, Y. Zhao, Z. H. Lu, Z. Yang, S. Hoogland and E. H. Sargent, *Science (80-.).*, 2017, **355**, 722–726.

10   N. J. Jeon, H. Na, E. H. Jung, T. Y. Yang, Y. G. Lee, G. Kim, H. W. Shin, S. Il Seok, J. Lee and J. Seo, *Nat. Energy*, 2018, **3**, 682–689.

11   Q. Lin, Z. Wang, L. M. Herz, H. J. Snaith, N. Sakai, F. P. Chmiel, Q. Lin, F. P. Chmiel, N. Sakai, L. M. Herz, H. J. Snaith, Z. Wang, L. M. Herz, H. J. Snaith, N. Sakai and F. P. Chmiel, *Nat. Energy*, 2017, **2**, 1–16.

12   G. Grancini, C. Roldán-Carmona, I. Zimmermann, E. Mosconi, X. Lee, D. Martineau, S. Narbey, F. Oswald, F. De Angelis, M. Graetzel and M. K. Nazeeruddin, *Nat. Commun.*, 2017, **8**, 15684.

13   D. Luo, W. Yang, Z. Wang, A. Sadhanala, Q. Hu, R. Su, R. Shivanna, G. F. Trindade, J. F. Watts, Z. Xu, T. Liu, K. Chen, F. Ye, P. Wu, L. Zhao, J. Wu, Y. Tu, Y. Zhang, X. Yang, W. Zhang, R. H. Friend, Q. Gong, H. J. Snaith and R. Zhu, *Science (80-.).*, 2018, **360**, 1442–1446.

14   X. Zhao, C. Yao, T. Liu, J. C. Hamill, G. O. Ngongang Ndjawa, G. Cheng, N. Yao, H. Meng and Y. -L. Loo, *Adv. Mater.*, 2019, **31**, 1904494.

15   X. Zhao, F. Zhang, C. Yi, D. Bi, X. Bi, P. Wei, J. Luo, X. Liu, S. Wang, X. Li, S. M. Zakeeruddin and M. Grätzel, *J. Mater. Chem. A*, 2016, **4**, 16330–16334.

16   J. H. Heo, S. H. Im, J. H. Noh, T. N. Mandal, C. S. Lim, J. A. Chang, Y. H. Lee, H. J. Kim,

A. Sarkar, M. K. Nazeeruddin, M. Grätzel and S. Il Seok, *Nat. Photonics*, 2013, **7**, 486–491.

17   M. M. Lee, J. Teuscher, T. Miyasaka, T. N. Murakami and H. J. Snaith, *Science (80-.).*, 2012, **338**, 643–647.

18   H. Min, M. Kim, S. U. Lee, H. Kim, G. Kim, K. Choi, J. H. Lee and S. Il Seok, *Science (80-.).*, 2019, **366**, 749–753.

19   Q. Jiang, Y. Zhao, X. Zhang, X. Yang, Y. Chen, Z. Chu, Q. Ye, X. Li, Z. Yin and J. You, *Nat. Photonics*, 2019, **13**, 460–466.

20   J. J. Yoo, S. Wieghold, M. C. Sponseller, M. R. Chua, S. N. Bertram, N. T. P. Hartono, J. S. Tresback, E. C. Hansen, J. P. Correa-Baena, V. Bulović, T. Buonassisi, S. S. Shin and M. G. Bawendi, *Energy Environ. Sci.*, 2019, **12**, 2192–2199.

21   J. Liu, Y. Wu, C. Qin, X. Yang, T. Yasuda, A. Islam, K. Zhang, W. Peng, W. Chen and L. Han, *Energy Environ. Sci*, 2014, **7**, 2963–2967.

22   H. D. Pham, T. T. Do, J. Kim, C. Charbonneau, S. Manzhos, K. Feron, W. C. Tsoi, J. R. Durrant, S. M. Jain and P. Sonar, *Adv. Energy Mater.*, 2018, **8**, 1703007.

23   W. Zhou, Z. Wen and P. Gao, *Adv. Energy Mater.*, 2018, **8**, 1702512.

24   J. A. Christians, P. Schulz, J. S. Tinkham, T. H. Schloemer, S. P. Harvey, B. J. Tremolet De Villers, A. Sellinger, J. J. Berry and J. M. Luther, *Nat. Energy*, 2018, **3**, 68–74.

25   C. Huang, W. Fu, C. Z. Li, Z. Zhang, W. Qiu, M. Shi, P. Heremans, A. K. Y. Jen and H. Chen, *J. Am. Chem. Soc.*, 2016, **138**, 2528–2531.

26   S. Paek, P. Qin, Y. Lee, K. T. Cho, P. Gao, G. Grancini, E. Oveisi, P. Gratia, K. Rakstys, S. A. Al-Muhtaseb, C. Ludwig, J. Ko and M. K. Nazeeruddin, *Adv. Mater.*, 2017, **29**, 1606555.

27   M. Cheng, B. Xu, C. Chen, X. Yang, F. Zhang, Q. Tan, Y. Hua, L. Kloo and L. Sun, *Adv. Energy Mater.*, 2015, **5**, 1401720.

28   Z. Li, Z. Zhu, C. C. Chueh, S. B. Jo, J. Luo, S. H. Jang and A. K. Y. Jen, *J. Am. Chem. Soc.*, 2016, **138**, 11833–11839.

29   E. H. Jung, N. J. Jeon, E. Y. Park, C. S. Moon, T. J. Shin, T. Y. Yang, J. H. Noh and J. Seo, *Nature*, 2019, **567**, 511–515.

30   X. Yin, J. Zhou, Z. Song, Z. Dong, Q. Bao, N. Shrestha, S. S. Bista, R. J. Ellingson, Y. Yan and W. Tang, *Adv. Funct. Mater.*, 2019, **29**, 1904300.

31   S. Wang, H. Chen, J. Zhang, G. Xu, W. Chen, R. Xue, M. Zhang, Y. Li and Y. Li, *Adv. Mater.*, 2019, **31**, 1903691.

32   G. Tumen-Ulzii, C. Qin, D. Klotz, M. R. Leyden, P. Wang, M. Auffray, T. Fujihara, T. Matsushima, J. W. Lee, S. J. Lee, Y. Yang and C. Adachi, *Adv. Mater.*, 2020, **32**, 1905035.

33   Q. Chen, H. Zhou, T. Bin Song, S. Luo, Z. Hong, H. S. Duan, L. Dou, Y. Liu and Y. Yang, *Nano Lett.*, 2014, **14**, 4158–4163.

34   K. T. Cho, S. Paek, G. Grancini, C. Roldán-Carmona, P. Gao, Y. Lee and M. K. Nazeeruddin, *Energy Environ. Sci.*, 2017, **10**, 621–627.

35   P. Chen, Y. Bai, S. Wang, M. Lyu, J. H. Yun and L. Wang, *Adv. Funct. Mater.*, 2018, **28**, 1706923.

36   Y. Cho, A. M. Soufiani, J. S. Yun, J. Kim, D. S. Lee, J. Seidel, X. Deng, M. A. Green, S. Huang and A. W. Y. Ho-Baillie, *Adv. Energy Mater.*, 2018, **8**, 1703392.

37   K. T. Cho, G. Grancini, Y. Lee, E. Oveisi, J. Ryu, O. Almora, M. Tschumi, P. A. Schouwink, G. Seo, S. Heo, J. Park, J. Jang, S. Paek, G. Garcia-Belmonte and M. K. Nazeeruddin, *Energy Environ. Sci.*, 2018, **11**, 952–959.

38   Y. Lin, Y. Bai, Y. Fang, Z. Chen, S. Yang, X. Zheng, S. Tang, Y. Liu, J. Zhao and J. Huang, *J. Phys. Chem. Lett.*, 2018, **9**, 654–658.

39   M. Abdi-Jalebi, Z. Andaji-Garmaroudi, S. Cacovich, C. Stavrakas, B. Philippe, J. M. Richter, M. Alsari, E. P. Booker, E. M. Hutter, A. J. Pearson, S. Lilliu, T. J. Savenije, H. Rensmo, G. Divitini, C. Ducati, R. H. Friend and S. D. Stranks, *Nature*, 2018, **555**, 497–501.

40   T. Niu, J. Lu, X. Jia, Z. Xu, M. C. Tang, D. Barrit, N. Yuan, J. Ding, X. Zhang, Y. Fan, T. Luo, Y. Zhang, D. M. Smilgies, Z. Liu, A. Amassian, S. Jin, K. Zhao and S. Liu, *Nano Lett.*, 2019, **19**, 7181–7190.

41   S. Y. Wang, C. P. Chen, C. L. Chung, C. W. Hsu, H. L. Hsu, T. H. Wu, J. Y. Zhuang, C. J. Chang, H. M. Chen and Y. J. Chang, *ACS Appl. Mater. Interfaces*, 2019, **11**, 40050–40061.

42   S. J. Park, S. Jeon, I. K. Lee, J. Zhang, H. Jeong, J. Y. Park, J. Bang, T. K. Ahn, H. W. Shin, B. G. Kim and H. J. Park, *J. Mater. Chem. A*, 2017, **5**, 13220–13227.

43   J. A. McCleverty and T. J. Meyer, *Comprehensive Coordination Chemistry II*, 2004, vol. 1–9.

44   X. Gu, Y. Li, Y. Mu, M. Zhang, T. Lu and P. Wang, *RSC Adv.*, 2018, **8**, 9409–9413.

45   S. H. Turren-Cruz, A. Hagfeldt and M. Saliba, *Science (80-.).*, 2018, **362**, 449–453.

46   X. X. Gao, W. Luo, Y. Zhang, R. Hu, B. Zhang, A. Züttel, Y. Feng and M. K. Nazeeruddin, *Adv. Mater.*, 2020, **32**, 1905502.

47   J. C. Hamill, J. C. Sorli, I. Pelczer, J. Schwartz and Y.-L. Loo, *Chem. Mater.*, 2019, **31**, 2114–2120.

48   C. Noël, S. Pescetelli, A. Agresti, A. Franquet, V. Spampinato, A. Felten, A. di Carlo, L. Houssiau and Y. Busby, *Materials (Basel).*, 2019, **12**, 726.

49   D. Wei, F. Ma, R. Wang, S. Dou, P. Cui, H. Huang, J. Ji, E. Jia, X. Jia, S. Sajid, A. M. Elseman, L. Chu, Y. Li, B. Jiang, J. Qiao, Y. Yuan and M. Li, *Adv. Mater.*, 2018, **30**, 1707583.

50   W. Zhang, S. Pathak, N. Sakai, T. Stergiopoulos, P. K. Nayak, N. K. Noel, A. A. Haghighirad, V. M. Burlakov, D. W. Dequilettes, A. Sadhanala, W. Li, L. Wang, D. S.

Ginger, R. H. Friend and H. J. Snaith, *Nat. Commun.*, 2015, **6**, 10030.

51   T. Wu, Y. Wang, X. Li, Y. Wu, X. Meng, D. Cui, X. Yang and L. Han, *Adv. Energy Mater.*, 2019, **9**, 1803766.

52   E. J. Baran, C. C. Wagner, M. Rossi and F. Caruso, *Zeitschrift fur Anorg. und Allg. Chemie*, 2000, **626**, 701–705.

53   S. I. Ali and Z. Murtaza, *Polyhedron*, 1985, **4**, 821–827.

54   R. E. Hester, *Chapter 6. Raman and infrared spectroscopy of concentrated electrolyte solutions and fused salts*, 1969, vol. 66.

55   A. Glatfelter, C. Dybowski, S. Bai, D. Kragten, M. J. Blake, S. Segarra and D. L. Perry, *Spectrochim. Acta - Part A Mol. Biomol. Spectrosc.*, 2009, **71**, 1922–1926.

56   T. Kirchartz, J. A. Márquez, M. Stolterfoht and T. Unold, *Adv. Energy Mater.*, 2020, 10, 1904134.

57   Q. Wang, E. Mosconi, C. Wolff, J. Li, D. Neher, F. De Angelis, G. P. Suranna, R. Grisorio and A. Abate, *Adv. Energy Mater.*, 2019, **9**, 1900990.

58   X. Zhao, L. Tian, T. Liu, H. Liu, S. Wang, X. Li, O. Fenwick, S. Lei and W. Hu, *J. Mater. Chem. A*, 2019, **7**, 1509–1518.

59   B. Krogmeier, F. Staub, D. Grabowski, U. Rau and T. Kirchartz, *Sustain. Energy Fuels*, 2018, **2**, 1027–1034.

60   A. Al-Ashouri, A. Magomedov, M. Roß, M. Jošt, M. Talaikis, G. Chistiakova, T. Bertram, J. A. Márquez, E. Köhnen, E. Kasparavičius, S. Levcenco, L. Gil-Escrig, C. J. Hages, R. Schlatmann, B. Rech, T. Malinauskas, T. Unold, C. A. Kaufmann, L. Korte, G. Niaura, V. Getautis and S. Albrecht, *Energy Environ. Sci.*, 2019, **12**, 3356–3369.

61   J. Haddad, B. Krogmeier, B. Klingebiel, L. Krückemeier, S. Melhem, Z. Liu, J. Hüpkes, S. Mathur and T. Kirchartz, *Adv. Mater. Interfaces*, 2020, **7**, 2000366.

62   C. Sun, Z. Wu, H. L. Yip, H. Zhang, X. F. Jiang, Q. Xue, Z. Hu, Z. Hu, Y. Shen, M. Wang, F. Huang and Y. Cao, *Adv. Energy Mater.*, 2016, **6**, 1501534.

63   Z. Wang, M. A. Kamarudin, N. C. Huey, F. Yang, M. Pandey, G. Kapil, T. Ma and S. Hayase, *ChemSusChem*, 2018, **11**, 3941–3948.

64   Y. Cao, Y. Li, T. Morrissey, B. Lam, B. O. Patrick, D. J. Dvorak, Z. Xia, T. L. Kelly and C. P. Berlinguette, *Energy Environ. Sci.*, 2019, **12**, 3502–3507.

65   L. Yang, F. Cai, Y. Yan, J. Li, D. Liu, A. J. Pearson and T. Wang, *Adv. Funct. Mater.*, 2017, **27**, 1702613.

66   J. C. Yu, J. A. Hong, E. D. Jung, D. Bin Kim, S. M. Baek, S. Lee, S. Cho, S. S. Park, K. J. Choi and M. H. Song, *Sci. Rep.*, 2018, **8**, 1070.

67   W. Chen, Y. Wu, J. Fan, A. B. Djurišić, F. Liu, H. W. Tam, A. Ng, C. Surya, W. K. Chan, D. Wang and Z. B. He, *Adv. Energy Mater.*, 2018, **8**, 1703519.

68   D. Bi, C. Yi, J. Luo, J. D. Décoppet, F. Zhang, S. M. Zakeeruddin, X. Li, A. Hagfeldt and M. Grätzel, *Nat. Energy*, 2016, **1**, 16142.

69   T. H. Schloemer, J. A. Christians, J. M. Luther and A. Sellinger, *Chem. Sci.*, 2019, **10**, 1904–1935.

70   M. V. Khenkin, E. A. Katz, A. Abate, G. Bardizza, J. J. Berry, C. Brabec, F. Brunetti, V. Bulović, Q. Burlingame, A. Di Carlo, R. Cheacharoen, Y.-B. Cheng, A. Colsmann, S. Cros, K. Domanski, M. Dusza, C. J. Fell, S. R. Forrest, Y. Galagan, D. Di Girolamo, M. Grätzel, A. Hagfeldt, E. von Hauff, H. Hoppe, J. Kettle, H. Köbler, M. S. Leite, S. Liu, Y.-L. Loo, J. M. Luther, C.-Q. Ma, M. Madsen, M. Manceau, M. Matheron, M. McGehee, R. Meitzner, M. K. Nazeeruddin, A. F. Nogueira, Ç. Odabaşı, A. Osherov, N.-G. Park, M. O. Reese, F. De Rossi, M. Saliba, U. S. Schubert, H. J. Snaith, S. D. Stranks, W. Tress, P. A. Troshin, V. Turkovic, S. Veenstra, I. Visoly-Fisher, A. Walsh, T. Watson, H. Xie, R. Yıldırım, S. M. Zakeeruddin, K. Zhu and M. Lira-Cantu, *Nat. Energy*, 2020, **5**, 35–49.

71   Z. Li, C. Xiao, Y. Yang, S. P. Harvey, D. H. Kim, J. A. Christians, M. Yang, P. Schulz, S. U. Nanayakkara, C. S. Jiang, J. M. Luther, J. J. Berry, M. C. Beard, M. M. Al-Jassim and K. Zhu, *Energy Environ. Sci.*, 2017, **10**, 1234–1242.

72   J. Schoonman, *Solid State Commun.*, 1973, **13**, 673–676.

73   E. J. Juarez-Perez, L. K. Ono, M. Maeda, Y. Jiang, Z. Hawash and Y. Qi, *J. Mater. Chem. A*, 2018, **6**, 9604–9612.

74   C. Qin, T. Matsushima, T. Fujihara, W. J. Potscavage and C. Adachi, *Adv. Mater.*, 2016, **28**, 466–471.

75   H. Cho, S. H. Jeong, M. H. Park, Y. H. Kim, C. Wolf, C. L. Lee, J. H. Heo, A. Sadhanala, N. S. Myoung, S. Yoo, S. H. Im, R. H. Friend and T. W. Lee, *Science (80-.).*, 2015, **350**, 1222–1225.

76   S. Bai, P. Da, C. Li, Z. Wang, Z. Yuan, F. Fu, M. Kawecki, X. Liu, N. Sakai, J. T. W. Wang, S. Huettner, S. Buecheler, M. Fahlman, F. Gao and H. J. Snaith, *Nature*, 2019, **571**, 245–250.

77   T. Malinauskas, M. Saliba, T. Matsui, M. Daskeviciene, S. Urnikaite, P. Gratia, R. Send, H. Wonneberger, I. Bruder, M. Graetzel, V. Getautis and M. K. Nazeeruddin, *Energy Environ. Sci.*, 2016, **9**, 1681–1686.

78   H. Zheng, G. Liu, C. Zhang, L. Zhu, A. Alsaedi, T. Hayat, X. Pan and S. Dai, *Sol. Energy*, 2018, **159**, 914–919.

79   M. C. Jung, S. R. Raga, L. K. Ono and Y. Qi, *Sci. Rep.*, 2015, **5**, 9863.

80   Z. Hawash, L. K. Ono, S. R. Raga, M. V. Lee and Y. Qi, *Chem. Mater.*, 2015, **27**, 562–569.

81   J. Zhang, T. Zhang, L. Jiang, U. Bach and Y. B. Cheng, *ACS Energy Lett.*, 2018, **3**, 1677–1682.

82   T. H. Schloemer, T. S. Gehan, J. A. Christians, D. G. Mitchell, A. Dixon, Z. Li, K. Zhu, J. J. Berry, J. M. Luther and A. Sellinger, *ACS Energy Lett.*, 2019, **4**, 473–482.

83   M. Saliba, T. Matsui, J. Y. Seo, K. Domanski, J. P. Correa-Baena, M. K. Nazeeruddin, S. M. Zakeeruddin, W. Tress, A. Abate, A. Hagfeldt and M. Grätzel, *Energy Environ. Sci.*, 2016, **9**, 1989–1997.

84   M. Deepa, M. Salado, L. Calio, S. Kazim, S. M. Shivaprasad and S. Ahmad, *Phys. Chem. Chem. Phys.*, 2017, **19**, 4069–4077.

85   Y. Hu, E. M. Hutter, P. Rieder, I. Grill, J. Hanisch, M. F. Aygüler, A. G. Hufnagel, M. Handloser, T. Bein, A. Hartschuh, K. Tvingstedt, V. Dyakonov, A. Baumann, T. J. Savenije, M. L. Petrus and P. Docampo, *Adv. Energy Mater.*, 2018, **8**, 1703057.

Metal halide perovskite solar cells (PSCs) with doped Spiro-OMeTAD as the hole-transport layer (HTL) have attracted much attention due to their high power-conversion efficiencies (PCEs), and the promise that they can be solution processed. However, the dopants and additives used with Spiro-OMeTAD can readily diffuse into the absorber and negatively affect the long-term stability of PSCs. To address this, many dopant-free small-molecule hole-transport materials (HTMs) have been reported, but the PCEs of such PSCs remain inferior to those using doped Spiro-OMeTAD, with little attention paid to the interactions between the HTL and the perovskite absorber in PSCs. We report a facile design concept to functionalize HTMs so they serve two functions: passivate perovskite surface defects to lower trap densities and enable efficient charge transfer and transport from the absorber to the anode without mobile dopants. PSCs with functionalized one particular such HTM exhibit a champion PCE of 22.4% and a substantively improved operational stability of T_{80} = 1617h for encapsulated cells tested under continuous illumination at 30 °C in air. This HTM design concept should benefit future interfacial engineering to further advance highly efficient and stable perovskite solar cells.